Structure and ESCRT-III protein interactions of the MIT domain of human VPS4A

Anna Scott, Jason Gaspar, Melissa D. Stuchell-Brereton, Steven L. Alam, Jack J. Skalicky, and Wesley I. Sundquist*

Department of Biochemistry, 20 N, 1900 E, University of Utah School of Medicine, Salt Lake City, UT 84132-3201

Edited by John M. Coffin, Tufts University School of Medicine, Boston, MA, and approved August 8, 2005 (received for review March 16, 2005)

The VPS4 AAA ATPases function both in endosomal vesicle formation and in the budding of many enveloped RNA viruses, including HIV-1. VPS4 proteins act by binding and catalyzing release of the membrane-associated ESCRT-III protein lattice, thereby allowing multiple rounds of protein sorting and vesicle formation. Here, we report the solution structure of the N-terminal VPS4A microtubule interacting and transport (MIT) domain and demonstrate that the VPS4A MIT domain binds the C-terminal half of the ESCRT-III protein, CHMP1B (K_d = 20 ± 13 μM). The MIT domain forms an asymmetric three-helix bundle that resembles the first three helices in a tetratricopeptide repeat (TPR) motif. Unusual interhelical interactions are mediated by a series of conserved aromatic residues that form coiled-coil interactions between the second two helices and also pack against the conserved alanines that interdigitate between the first two helices. Mutational analyses revealed that a conserved leucine residue (Leu-64) on the third helix that would normally bind the fourth helix in an extended TPR is used to bind CHMP1B, raising the possibility that ESCRT-III proteins may bind by completing the TPR motif.

HIV | budding | vacuolar protein sorting | multivesicular body | NMR

Proteins targeted for lysosomal degradation are sorted into vesicles that bud into late endosomal compartments called multivesicular bodies (MVB). Once formed, multivesicular bodies can undergo several different fates, either serving as long-term storage compartments, fusing with lysosomes to deliver the internal vesicles and their contents for degradation, or fusing with the plasma membrane to release the vesicles as extracellular "exosomes." The MVB functions in a number of important biological processes, including receptor down-regulation, antigen presentation, intercellular communication, and development (for reviews, see refs. 1–4). Moreover, a number of enveloped RNA viruses, including HIV-1, usurp cellular proteins involved in MVB biogenesis to facilitate virus budding, a process that shares many similarities with MVB vesicle formation (5, 6).

MVB vesicle formation and protein sorting require a complex set of protein machinery (the class E proteins) originally identified in yeast genetic screens (2, 7). Subsequent studies have identified at least one human homolog for every yeast class E protein (5), indicating that the MVB pathway is conserved across eukaryotes. Most class E proteins function as components of one of three endosomal sorting complexes required for transport (ESCRT-I, -II, and -III), which are sequentially recruited to sites of MVB protein sorting and vesicle formation (8). The ESCRT-III proteins are the last to assemble, and are thought to form a membrane-associated lattice that functions in the final stages of protein sorting and vesicle formation (2, 8). Humans have a total of 10 ESCRT-III-like proteins (the "CHMP" proteins) that can be subdivided into six families corresponding to the six ESCRT-III proteins in yeast (5, 9). Four of the ESCRT-III protein families (corresponding to CHMP-2, -3, -4, and -6) are considered core ESCRT-III components, whereas the other two families (CHMP-1 and CHMP-5) may play regulatory or peripheral roles (8). The ESCRT-III proteins, in turn, recruit the VPS4 AAA ATPases to sites of MVB vesicle formation (10). This recruitment appears to occur through direct protein–protein interactions, because both human and yeast ESCRT-III proteins bind directly to VPS4 proteins (11–13). Subsequent release of ESCRT complexes from the membrane requires the ATPase activity of the VPS4 proteins (9, 10, 14–17). Thus, the VPS4 ATPases allow the ESCRT machinery to recycle through multiple rounds of vesicle formation and may also provide the energy necessary for protein sorting and/or vesicle formation.

Humans and other mammals have two highly related VPS4 proteins (designated VPS4A and VPS4B/SKD1) that are 80% identical to one another and ≈60% identical to the yeast VPS4 protein (17). Like other AAA ATPases, the VPS4 proteins have modular structures, with an N-terminal substrate recognition domain preceding the canonical AAA ATPase cassette (Fig. 1) (18, 19). Although the catalytic domains are highly conserved, distinct substrate specificities are created through the use of different N-terminal domains. The N-terminal domains of the VPS4 proteins belong to a family called MIT (microtubule interacting and trafficking) domains (20, 21). MIT domains are found in other AAA ATPases, such as spastin, and are also present in proteins that lack ATPase domains, such as SNX15 and PalB/calpain-7. Several recent yeast two-hybrid studies have indicated that at least some MIT domains may act as protein recognition modules that bind ESCRT-III/CHMP proteins (13, 22). However, detailed biochemical or structural analyses have not yet been performed for any MIT domain. Here, we describe the structure and protein–protein interactions of the VPS4A MIT domain.

Experimental Procedures

Supporting Information. Further details can be found in Tables 1 and 2 and Figs. 5–7, which are published as supporting information on the PNAS web site.

MIT Domain Alignments. The MIT domain sequence alignment (Fig. 1) matches that presented previously (21, 23), except that the third helices in spastin, spartin, and tobacco mosaic virus (TMV) helicase were manually adjusted by first aligning spastin with VPS4A and VPS4B by using CLUSTALW (24), and then aligning spartin and TMV helicase with spastin. This procedure optimized the alignment of highly conserved residues without altering the 50% consensus sequence.

Cloning. DNA encoding VPS4A residues 1–84, 1–122, or 1–437 (full length) or VPS4B 1–129 or 1–444 (full length) was amplified from EST templates (ATCC 81449 and 6216963) (25). The 5′ PCR primer also reintroduced the first five amino acids that were missing from the VPS4A EST sequence. DNA fragments were cloned into NdeI/BamH1 sites of pET16b (Novagen), modified

This paper was submitted directly (Track II) to the PNAS office.

Abbreviations: MVB, multivesicular body; TPR, tetratricopeptide repeats.

Data deposition: The model coordinates and assignments have been deposited in the Protein Data Bank, www.pdb.org (PDB ID code 1YXR).

*To whom correspondence should be addressed. E-mail: wes@biochem.utah.edu.

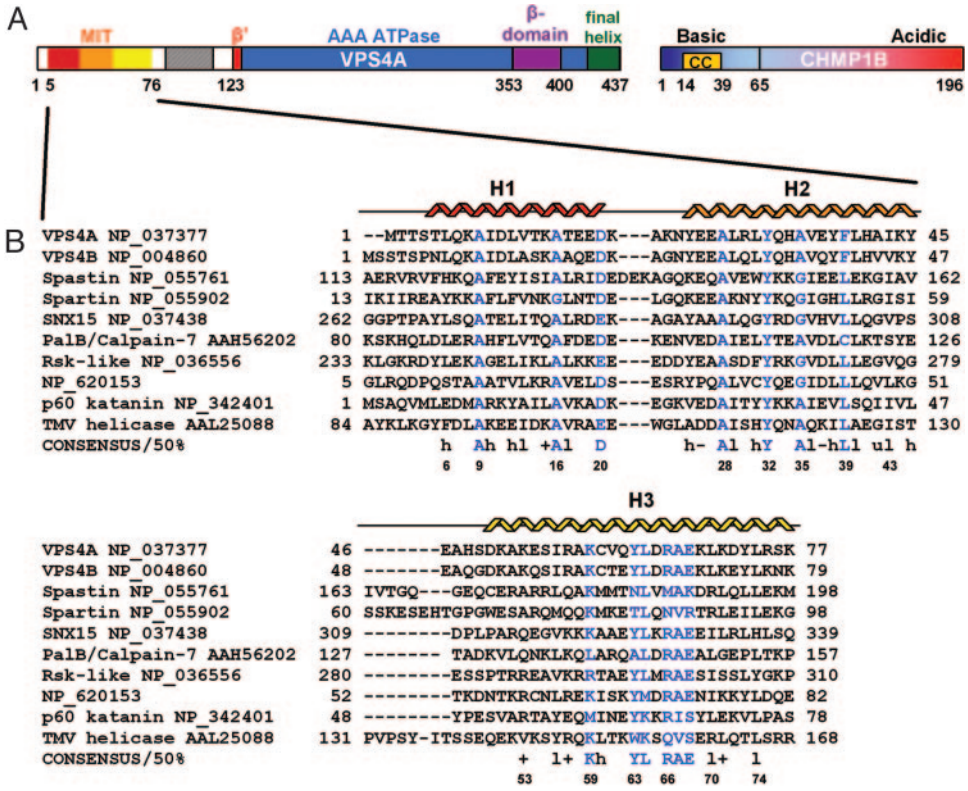

Fig. 1. Sequences and features of VPS4A, CHMP1B, and MIT domains. (*A*) Schematic illustrations of human VPS4A (19) and CHMP1B. The predicted coiled-coil (CC) of CHMP1B was identified at a probability of 0.17 by using MULTICOIL (41). (*B*) Sequence alignment of known MIT domains from eight human proteins (*Upper*) and two proteins lacking human homologs. The ''consensus'' sequence (*Lower*) was derived from all 116 MIT domains in the SMART database (23). Highly conserved residues (>50% identity) are shown in blue, and residue types conserved in >50% of the sequences are shown in lowercase (h, hydrophobic; +, positively charged; -, negatively charged; u, Ala or Gly; l, Ile, Val, or Leu). Numbering corresponds to VPS4A.

to encode a TEV protease site after the N-terminal His-10 tag. Site directed mutants were created by using the QuikChange method (Stratagene). DNA fragments encoding CHMP1B residues 65–196 and 1–196 (full length) were amplified from a HeLa cDNA library (Stratagene) (26), and cloned into the NdeI/BamHI sites of a modified pGEX2T vector that encoded a TEV protease cleavage site. All constructs were verified by DNA sequencing.

Protein Expression and Purification. Protein expression and purification protocols were similar for the different VPS4 proteins, and are described for $VPS4A_{1–122}$. His-10-$VPS4A_{1–122}$ was expressed in 2-liter cultures of BL21(DE3) *Escherichia coli* cells grown in LB or in M9 media supplemented with either 2 g/liter $^{15}NH_4Cl$ or 2 g/liter $^{15}NH_4Cl$ and 2 g/liter $^{13}C_6$-glucose. Expression was induced (4 h at 27°C) with 0.5 mM IPTG (A_{600} = 0.65). Subsequent steps were performed at 4°C. Cells were harvested and resuspended in lysis buffer (50 mM Tris, pH 8.0/50 mM imidazole/500 mM NaCl) supplemented with protease inhibitors (Roche Diagnostics) and lysed with 1 mg/ml lysozyme followed by sonication. The lysate was clarified by centrifugation (45 min, 35,000 × *g*), and the soluble protein purified by nickel Sepharose chromatography (Amersham Pharmacia). His-10-$VPS4A_{1–122}$ eluted at ≈400 mM imidazole from a linear gradient of 50–750 mM imidazole in lysis buffer. Protein fractions were pooled and dialyzed sequentially against two changes of cleavage buffer (20 mM Tris·HCl, pH 8.0/100 mM NaCl/5 mM EDTA), with 1 mM DTT replacing EDTA in the second change. The His-10 tag was removed by incubation with TEV protease (1 mg per 100 mg of protein, 12 h, 27°C) followed by anion exchange chromatography (Q Sepharose, Amersham Pharmacia). Flow-through fractions containing $VPS4A_{1–122}$ were concentrated to ≈4 ml, and the protein was purified to homogeneity by gel filtration chromatography (S75, Amersham Pharmacia). This procedure typically yielded ≈30 mg of $VPS4A_{1–122}$. TEV cleavage left two nonnative residues at the N terminus (Gly–His), which are not included in our numbering scheme. The protein was verified by N-terminal sequencing (G-H-M-T-T-S-T) and electrospray mass spectrometry ($MW_{exp.}$ = 14,168 Da, $MW_{calc.}$ = 14,167 Da).

GST Pull-Down Experiments. *E. coli* (30-ml cultures) expressing either GST or GST-$CHMP1B_{65–196}$ were pelleted, resuspended in 5 ml of lysis buffer (50 mM Tris·HCl, pH 7.4/50 mM NaCl/5 mM 2-mercaptoethanol), and lysed with 75 μl of 10 mg/ml lysozyme (20 min, 4°C) followed by addition of 100 μl of 5% deoxycholate (20 min) and sonication. Soluble proteins were collected after centrifugation for 45 min at 13,200 × *g*. Binding reactions (1 h at 4°C) contained 35 μM GST or GST-$CHMP1B_{65–196}$, 60 μM VPS4A or 300 μM $VPS4A_{1–84}$, and 100 μl glutathione agarose slurry (Amersham Pharmacia) in 190 ml total volume buffer (20 mM Tris·HCl, pH 8.0/100 mM NaCl/2 mM $MgCl_2$/2 mM $CaCl_2$/5 mM 2-mercaptoethanol/0.02% Nonidet P-40/5% glycerol). Unbound proteins were removed in three 1.2-ml buffer washes. Bound proteins were eluted from the matrix by boiling in 100 μl of 2× SDS/PAGE buffer and detected by SDS/PAGE.

Biosensor Binding Experiments. Biosensor binding experiments used a BIACORE 2000 with research-grade CM4 sensor chips. Approximately 5 kRU of anti-GST Ab was immobilized by amine-coupling, and GST-CHMP proteins or GST alone (ref-

erence) were captured in running buffer (≈0.5 kRU, 20 mM Tris, pH 8.0/100 mM NaCl/1 mM DTT/0.2 mg/ml BSA/0.005% P20). GST-CHMP proteins were either purified by glutathione affinity chromatography or captured directly from soluble *E. coli* lysates (no difference in binding was noted). Purified VPS4A MIT proteins were injected in running buffer (0–450 μM, 50 μl/min, 20°C). Data were collected at 2 Hz during 30-s association and dissociation phases and equilibrium binding isotherms fit to simple 1:1 binding models (27). VPS4A MIT proteins in running buffer were injected in duplicate or triplicate. Sensorgrams for wild-type $VPS4A_{1–84}$ and L64A mutant $VPS4A_{1–84}$ binding immobilized GST-$CHMP1B_{65–196}$ are given in Fig. 7*B*.

NMR Spectroscopy. NMR samples were 3 mM protein in 20 mM sodium phosphate (pH 5.5), 50 mM NaCl, 90% H_2O/10% D_2O. Spectra were recorded at 25°C on a Varian Inova 600 NMR spectrometer equipped with a triple-resonance $^1H/^{13}C/^{15}N$ probe and *z* axis pulsed-field gradients. Data were processed with FELIX (Accelrys, San Diego), and resonances were assigned by using standard approaches within the SPARKY program (T. D. Goddard and D. G. Kneller, University of California, San Francisco) (see Tables 1 and 2). Complete resonance assignments were obtained, with eight exceptions: H48 H^N, F39 H^ζ, K83 H^γ H^δ H^ε, and M1, M114, and M119 H^ε. Stereospecific assignments were obtained from GLOMSA (28) for six pairs of methylene protons: E18H^β, E18H^γ, N24H^β, E27H^β, Y38H^β, and E39H^β. Backbone torsion angles were estimated from ^{13}C chemical shifts by using TALOS (42). All prolines were in the *trans* conformation, as confirmed by intense Xxx(H^α)-Pro($H\delta$) sequential NOESY cross peaks and $^{13}C^\beta$ and $^{13}C^\gamma$ chemical shifts typical of *trans*-Pro (29).

Structure Calculations. NOE coordinates and intensities were obtained by using the tools in SPARKY. NOE assignments were obtained and initial structures calculated by using automated NOE assignment together with torsion angle dynamics as implemented in CYANA (28). A total of 100 randomized conformers were "folded" into 3D structures by introducing NOE constraints in a step-wise manner by using the criteria of chemical shift agreement, network anchoring, and consistency with an initial fold. Each conformer was subjected to 10,000 steps of torsion angle dynamics per cycle (seven cycles). The 20 structures with the lowest final CYANA target function values were then subjected to restrained energy minimization in CNS (30) using the final CYANA NOE and torsion angle constraints, as well as helical hydrogen bond restraints based upon chemical shift indices and local NOE patterns (Fig. 5). Structures were validated by using PROCHECK-NMR and AQUA (31) and visualized by using PYMOL (DeLano Scientific).

Results and Discussion

VPS4A MIT Domain Structure Determination. N-terminal fragments of VPS4A and VPS4B were screened for their feasibility for NMR structural studies. The two fragments tested, $VPS4A_{1–122}$ and $VPS4B_{1–129}$, were designed to span the entire region of VPS4B that was disordered in our recent crystal structure of the full-length protein (residues 1–122) (19). Both $VPS4A_{1–122}$ and $VPS4B_{1–129}$ exhibited reasonable amide proton and nitrogen chemical shift dispersion, but $VPS4B_{1–129}$ NH resonance linewidths and intensities varied, whereas the $VPS4A_{1–122}$ spectrum was of uniformly high quality. Therefore, this protein was selected for high-resolution structural studies.

Essentially complete proton resonance assignments were obtained for $VPS4A_{1–122}$ by using a standard suite of NMR experiments (Table 1). Analyses of short- and medium-range NOE patterns, $^3J_{HNHA}$ couplings, and ^{13}C chemical shift indices indicated the presence of three well defined helices (residues 5–20, 25–45, and 50–76), a fourth region with helical propensity (105–114), and random coil secondary structure elsewhere (Fig. 5). $VPS4A_{1–122}$ residues 77–122, including the final nascent helix, lacked any detectable long-range NOEs, and were therefore excluded from structure calculations. VPS4 residues 5–76 formed a tightly packed, well ordered structure as judged by the excellent agreement between different structures (0.26-Å backbone heavy atom rms deviation for 20 calculated structures), good geometries, low residual energies, and a lack of NOE violations (see Table 2 and Fig. 6).

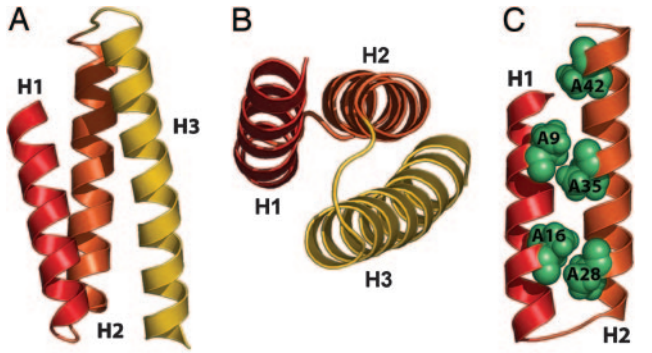

Fig. 2. $VPS4A_{5–76}$ MIT domain structure. (*A*) Ribbon diagram of the VPS4A MIT domain (residues 5–76). (*B*) View down the three helix bundle of the MIT domain, emphasizing the asymmetry in the disposition of the three helices. (*C*) "Alanine zipper" connecting $VPS4A_{5–76}$ MIT helices 1 and 2. The five conserved alanine side chains within this motif are shown explicitly.

Structure of the VPS4A MIT Domain. The MIT domain of VPS4A (residues 5–76) forms an antiparallel three helix bundle (Fig. 2*A*). The three helices wrap with a left superhelical twist, and are disposed asymmetrically onto three corners of a square (Fig. 2*B*). The third helix is longer than the first two, and has an ≈10° bend centered about residue Tyr-63. Helices 2 and 3 form a two-stranded, antiparallel coiled coil, and interact with canonical "knobs in holes" side chain interactions (32, 33) (Fig. 3). This interaction explains the predicted coiled-coil propensity of the third helix (10), and also explains the conservation of hydrophobic residues across MIT domains at helix 2 positions 25, 29, 32, 36, 39, and 43 and helix 3 positions 56, 60, 63, 67, 70, and 74 (see Fig. 1), because these residues correspond to the alternating **a** (+1) and **d** (+4) positions in the heptad repeats of the coiled coil. However, the coiled coil formed between helices 2 and 3 is unusual in that it is mediated by conserved aromatic (as opposed to aliphatic) side chains at positions 25, 32, 39, and 63.

In contrast, helices 1 and 2 do not form a canonical coiled coil, but rather interact through a motif that could be described as an "alanine zipper." As shown in Figs. 2*C* and 3, the closest contacts between the two helices are mediated by five alanine residues, two from helix 1 (Ala-9 and Ala-16), and three from helix 2 (Ala-28, Ala-35, and Ala-42). Each set of alanines is separated by seven residues, and the side chains therefore project from the same side of the helix with a spacing of two helical turns. However, unlike the side chains in a coiled coil, the alanines project directly toward the partner helix, and form an interdigitating strip between the two helices (Fig. 2*C*). As shown in Fig. 3, all of these alanines sit between hydrophobic residues that project from the +4 and +5 positions on the partner helix (numbering relative to the preceding alanine). The distance between helices 1 and 2 in the MIT domain of VPS4A is not unusual (≈10 Å), but this packing distance can only readily accommodate small side chains such as Ala and Gly at the five zipper positions (9, 16, 28, 35, and 42). Importantly, these alanines or glycines are highly conserved, particularly within the center of the zipper, with ≥93% conservation of Ala or Gly at

BIOCHEMISTRY

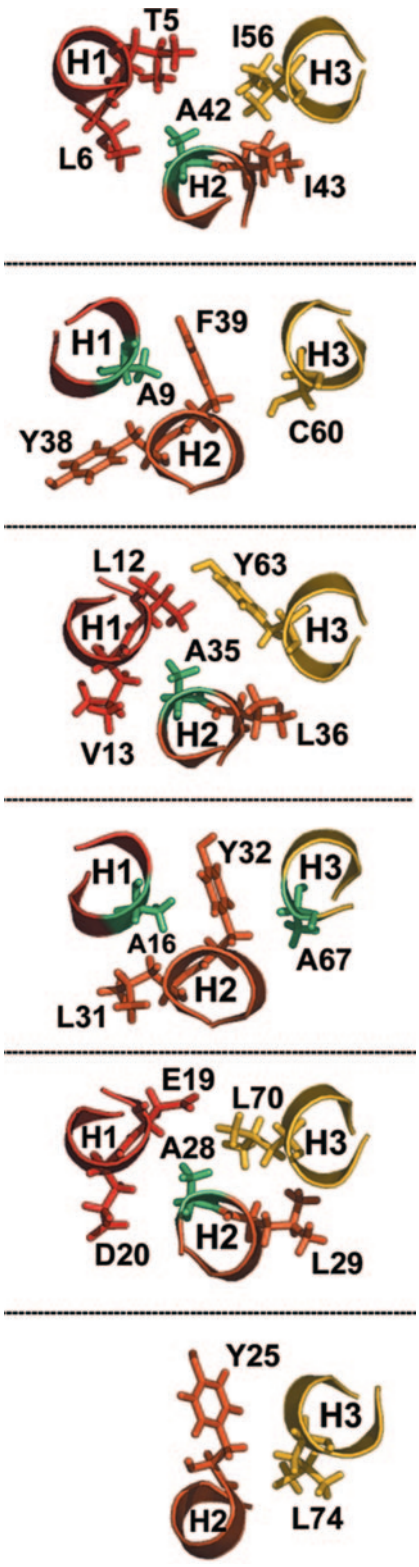

Fig. 3. Side chain interactions at the different layers of the VPS4A MIT three-helix bundle. Sequential amino acid layers in the three helix bundle of the VPS4A MIT domain. Note that side chain interactions between helices 2 (H2) and 3 (H3) follow canonical alternating ''knobs into holes'' interactions between residues at helix positions +1 (A) and +4 (D), whereas side chain packing between helices 1 (H1) and 2 (H2) is different because alternating alanine residues (highlighted in green) project almost directly at the pairing helix and are sandwiched between hydrophobic side chains from the +4 and +5 positions (relative to the preceding alanine) in the pairing helix.

positions 9, 16, 28, and 35 in the 116 known MIT domain sequences (23). Therefore, analogous interhelical packing interactions likely exist in all MIT domains.

Importantly, the alanine zipper formed between the first two helices is linked structurally to the aromatic coiled coil formed between the second two helices, so that the entire three-helix bundle of the MIT domain can be considered a single structural motif. Specifically, the two alanines from helix 1 (Ala-9 and Ala-16) pack between conserved central aromatic residues from helix 2 (Tyr-32 and Phe-39). Similarly, the three alanines on helix 2 (Ala-28, Ala-35, and Ala-42) pack against aromatic/large hydrophobic side chains from the heptad repeat of helix 3 (Leu-70, Tyr-63, and Ile-56). Thus, the central strip of aromatic residues between helices 2 and 3 simultaneously buttresses the alanine zipper and participates in coiled-coil formation, and apparently serves to hold the three helices at a proper angle (see Figs. 2*B* and 3).

The closest known structural matches to the VPS4A MIT domain occur for two distinct classes of helical bundles (34). The first class corresponds to the first three helices within canonical four helix bundles. In the best matches, the three MIT domain helices align with the first three helices of the four helix bundles with backbone atom rms deviations of ≈2 Å (e.g., α-1 catenin; Protein Data Bank ID 1h6g, Dali *z* score = 8.1, backbone atom rms deviation = 2.0 over 74 residues). However, as emphasized above, the interhelical side chain packing interactions of the $VPS4A_{5–76}$ MIT domain are quite distinct from those of canonical four helix bundles, and it therefore seems unlikely that MIT domains bind their partners by completing the four helix bundle. The second class of similar structures correspond to helices within tetratricopeptide repeats (TPR). For example, the three MIT domain helices align well with the first three helices in the TPR of FKBP51 (Protein Data Bank ID 1kt0, Dali *z* score = 8.7, backbone atom rms deviation = 2.1 over 70 residues in helices 1–3, see Fig. 4 *D* and *E*). TPR motifs are repeats of paired helices composed of two different types of interhelical interactions: an A/B interaction within each helical pair and a B/A′ interaction that links one helix pair to the next (35). TPR and MIT domain helices are similar in that: (*i*) the helices have similar spatial dispositions, (*ii*) an Ala/Gly zipper pairs the first two helices (the A/B interaction), and (*iii*) conserved aromatic residues perform similar roles in helping to bridge the first helix pair and the following repeat (the B/A′ interaction). In a TPR, the fourth (B′) helix, which is absent in the MIT domain, binds the third helix and we envision that an analogous interaction could mediate the intermolecular interaction with CHMP1B (see below).

The VPS4A MIT Domain Binds the C-Terminal Region of CHMP1B. To begin to define how the VPS4 ATPases interact with the assembled ESCRT-III lattice, we mapped the sites of interaction between the VPS4A and CHMP1B proteins. The 10 different human CHMP proteins exhibit only modest pairwise sequence identities (12–65%), but nevertheless share a number of common features, including similar sizes (210 ± 20 residues), predicted coiled-coil motifs, and highly asymmetric charge distributions (9). CHMP1B is typical of other CHMP proteins in that the first 64 residues are highly basic [predicted isoelectric point (PI) of 10.1] and contain a predicted coiled coil (see Fig. 1), whereas the C-terminal 132 residues are highly acidic (predicted PI of 4.5) and lack predicted coiled-coil motifs. We have previously used GST pull-down assays to demonstrate that both VPS4A and VPS4B bind to a series of full-length ESCRT-III proteins, including CHMP1B (12). As shown in Fig. 4*A*, the full-length recombinant VPS4A protein also bound a C-terminal fragment of GST-CHMP1B (residues 65–196), but not GST alone (compare lanes 4 and 5). Thus, VPS4A does not interact with the CHMP1B coiled-coil/basic region as had been pre-

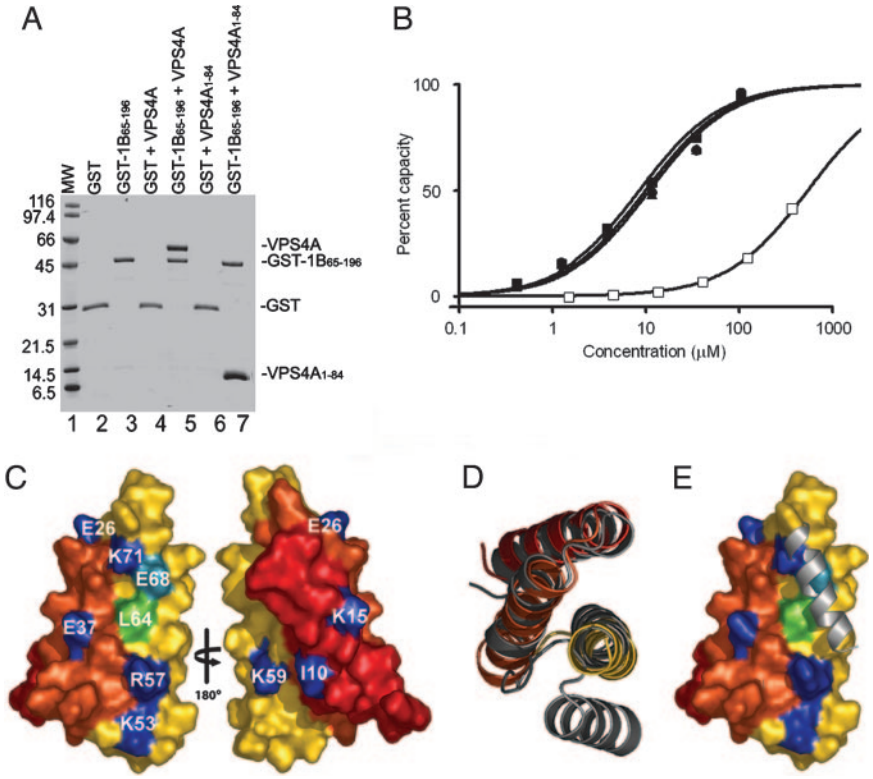

Fig. 4. Interactions between VPS4A and CHMP1B proteins. (*A*) GST pull-downs demonstrating that both full-length VPS4A and its isolated MIT domain ($VPS4A_{1–84}$) bind GST-$CHMP1B_{65–196}$ (denoted GST-$1B_{65–196}$, lanes 5 and 7) but not GST alone (lanes 4 and 6). Molecular weight standards (MW, lane 1), pure GST (lane 2), and pure GST-$CHMP1B_{65–196}$ (lane 3) are shown for reference. (*B*) Biosensor binding isotherms showing wild-type (WT) and L64A mutant $VPS4A_{1–84}$ proteins binding GST-CHMP1B and GST-$CHMP1B_{65–196}$. Filled circles, WT $VPS4A_{1–84}$ binding full-length GST-CHMP1B captured from *E. coli* extracts; filled triangles, WT $VPS4A_{1–84}$ binding GST-$CHMP1B_{65–196}$ captured from *E. coli* extracts; filled squares, WT $VPS4A_{1–84}$ binding affinity purified GST-$CHMP1B_{65–196}$; open squares, $VPS4A_{1–84}$ L64A binding affinity purified GST-$CHMP1B_{65–196}$. Binding to the GST control surface was negligible (not shown). Dissociation constants (μM) for WT $VPS4A_{1–84}$ binding were: CHMP1B = 20 ± 13 and $CHMP1B_{65–196}$ = 13 ± 6 μM; and were >500 μM for $VPS4A_{1–84}$ L64A binding to both constructs (minimum three independent measurements). (*C*) VPS4A MIT surface renderings showing the locations and identities of conserved residues. Conserved residues are color-coded based on the reduction in $CHMP_{65–196}$ binding affinity for alanine substitution mutations: dark blue, <3-fold change; light blue, 3- to 30-fold reduction; green, >30-fold reduction. Dissociation constants were: WT, 13 ± 6 μM; I10A, 17 ± 1 μM; K15A, 14 ± 1 μM; E26A, 8 ± 1 μM; E37A, 16 ± 2 μM; K53A, 20 ± 2 μM; R57A, 34 ± 4 μM; K59A, 9 ± 1 μM; L64A, >500 μM; E68A, 55 ± 4 μM; K71A, 18 ± 2 μM (minimum of two independent measurements). (*D*) Overlays of the first four helices of the TPR domain of FKBP51 (gray) with the MIT domain of VPS4A. The overlay shows the similarity of the structures and the position of the second paired helix (fourth overall) in the FKBP51 TPR domain, which is missing in the VPS4A MIT domain. (*E*) Side view of the overlay in *D*, but with the VPS4A MIT domain shown in a space filling model and color coded as in *C*. The figure emphasizes that residues required for CHMP1B binding (green, light blue) map to the same surface as the binding site for the second paired helix of the FKBP51 TPR domain.

dicted (10), but instead binds the protein's acidic C-terminal region. These data are consistent with other recent experiments showing that C-terminal regions of other CHMP proteins bind VPS4 in extracts (13, 36).

As discussed above, the ESCRT-III proteins are apparently substrates for the VPS4 ATPases (9, 10, 14–17) and AAA ATPase substrate recognition is typically meditated by the N-terminal domain (reviewed in ref. 18). Therefore, we tested whether the N-terminal MIT domain of VPS4A alone ($VPS4A_{1–84}$) could bind CHMP1B proteins. As shown in Fig. 4*A*, $VPS4A_{1–84}$ bound GST-$CHMP1B_{65–196}$, but not GST alone (compare lanes 6 and 7). Thus, the VPS4A MIT domain alone contains CHMP1B binding activity. This observation was confirmed and quantitated in biosensor binding experiments, in which soluble monomeric $VPS4A_{1–84}$ bound specifically to immobilized GST-CHMP1B proteins. VPS4A MIT domain binding and dissociation were rapid at 20°C, and dissociation constants were therefore obtained by analyzing equilibrium binding phases (see Fig. 7*B* for representative sensorgrams). As shown in Fig. 4*B*, the MIT domain bound with equal affinity to both full-length GST-CHMP1B (K_d = 20 ± 13 μM) and GST-$CHMP1B_{65–196}$ (K_d = 13 ± 6 μM). Thus, a C-terminal CHMP1B fragment that contains the acidic region but lacks the predicted coiled-coil contributes all of the energetically significant VPS4A MIT binding contacts.

Biosensor binding assays were also used to map the interaction surface on the VPS4A MIT domain. We reasoned that the binding site might feature a cluster of conserved, surface-exposed residues, particularly hydrophobic residues. As discussed above, interhelical packing interactions rationalize the conservation of all hydrophobic residues found with >50% frequency in the MIT domain, with the sole exception of Leu-64, which is exposed on the surface of helix 3 (see Figs. 1 and 4*C*). Most of the remaining hydrophobic residues that lack strict sequence conservation also appear to perform structural roles, as do a conserved pair of charged residues, Asp-20 and Arg-66, which approach one another across the interface between helices 1 and 2, where they may interact to form a salt bridge. This leaves nine solvent-exposed residues that are conserved at >50% identity and that appear unlikely to perform important structural roles within the three helix bundle (Lys/Arg-15, Glu/Asp-26, Glu/Asp-37, Arg/Lys-53, Arg/Lys-57, Lys-59, Leu-64, Glu-68, and Lys/Arg-71). We created an ensemble of proteins that contained single alanine substitution mutations at each conserved position, as well as in the exposed Ile-10 residue. Al-

though Ile-10 is <50% conserved across all MIT domains, this position is typically hydrophobic and lies on the face opposite Leu-64.

As summarized in Fig. 4 *B–E*, the affinity of CHMP1B (and $CHMP1B_{65–96}$) binding was reduced very substantially (>30-fold) by the $VPS4A_{1–84}$ L64A mutation. An alanine substitution mutation in the adjacent Glu-68 residue also reduced CHMP1B binding affinity, albeit modestly (3.5-fold). None of the other mutants altered the CHMP1B binding affinity significantly (<3-fold). Importantly, an [^{1}H,^{15}N] HSQC spectrum of the $VPS4A_{1–84}$ L64A protein confirmed that this mutation did not alter the overall fold of the MIT domain (see Fig. 7*A*). Therefore, we conclude that CHMP1B contacts the Leu-64/Glu-68 patch directly. As shown in Fig. 4*E*, this patch corresponds to the surface of helix 3 that would normally interact with the fourth helix in a TPR motif. Thus, the short TPR in the MIT domain has adapted to bind a target protein in trans, rather than a fourth helix in cis, raising the intriguing possibility that helices from the ESCRT-III proteins may bind by completing or extending the TPR.

Potential Biological Implications. MIT domains are found in proteins that function in important biological processes such as endosomal protein sorting (VPS4, SNX15, spastin) (10, 20, 22), virus budding (VPS4) (25), microtubule organization (spastin) (21, 22, 37, 38), and maintenance of motor neuron function (spastin and spartin) (22, 39). The general conservation of key structural residues indicates that all MIT domains will form three-helix bundles that are similar to the VPS4A MIT domain structure presented here.

Our data also demonstrate that the MIT domain of VPS4A binds directly to the C-terminal acidic region of the ESCRT-III protein, CHMP1B, and to analogous regions on other human CHMP proteins (data not shown). These interactions seem functionally important because recruitment of VPS4 proteins to endosomal membranes requires both the C-terminal half of CHMP proteins (40) and the MIT domains of VPS4 proteins (10). Interestingly, another MIT domain-containing protein, spastin, is also a CHMP1B-binding protein and the MIT domain is again required for this interaction (22). As shown in Fig. 1, the key Leu-64 residue in helix 3 critical for the VPS4A/CHMP1B interaction is also conserved in the spastin MIT domain. This domain again precedes a AAA ATPase cassette, raising the possibility that spastin may perform at least some functions that are analogous to those of the two better characterized human VPS4 proteins. Indeed, although the binding partners for most MIT domain proteins have not yet been determined experimentally, the apparent conservation of the exposed leucine on helix 3 suggests that other human MIT domain proteins such as SNX15, which again seems to function in endosomal protein sorting (20), may also interact functionally with ESCRT-III proteins.

We thank Tom Alber for helpful discussions on helical packing interactions, Darrell Davis for his efforts on behalf of the University of Utah Biomolecular NMR Center, and David Myszka and Phini Katsamba for performing the biosensor binding experiments. This work was funded by National Institutes of Health Grant AI51174 (to W.I.S.).

1. Murk, J. L., Stoorvogel, W., Kleijmeer, M. J. & Geuze, H. J. (2002) *Semin. Cell Dev. Biol.* **13,** 303–311.
2. Katzmann, D. J., Odorizzi, G. & Emr, S. D. (2002) *Nat. Rev. Mol. Cell Biol.* **3,** 893–905.
3. Gruenberg, J. & Stenmark, H. (2004) *Nat. Rev. Mol. Cell Biol.* **5,** 317–323.
4. de Gassart, A., Geminard, C., Hoekstra, D. & Vidal, M. (2004) *Traffic* **5,** 896–903.
5. Morita, E. & Sundquist, W. I. (2004) *Annu. Rev. Cell Dev. Biol.* **20,** 395–425.
6. Demirov, D. G. & Freed, E. O. (2004) *Virus Res.* **106,** 87–102.
7. Raymond, C. K., Howald-Stevenson, I., Vater, C. A. & Stevens, T. H. (1992) *Mol. Biol. Cell* **3,** 1389–1402.
8. Babst, M., Katzmann, D., Estepa-Sabal, E., Meerloo, T. & Emr, S. (2002) *Dev. Cell* **3,** 271–282.
9. Howard, T. L., Stauffer, D. R., Degnin, C. R. & Hollenberg, S. M. (2001) *J. Cell Sci.* **114,** 2395–2404.
10. Babst, M., Wendland, B., Estepa, E. J. & Emr, S. D. (1998) *EMBO J.* **17,** 2982–2993.
11. Martin-Serrano, J., Yaravoy, A., Perez-Caballero, D. & Bieniasz, P. D. (2003) *Proc. Natl. Acad. Sci. USA* **100,** 12414–12419.
12. von Schwedler, U. K., Stuchell, M., Muller, B., Ward, D. M., Chung, H. Y., Morita, E., Wang, H. E., Davis, T., He, G. P., Cimbora, D. M., *et al.* (2003) *Cell* **114,** 701–713.
13. Yeo, S. C., Xu, L., Ren, J., Boulton, V. J., Wagle, M. D., Liu, C., Ren, G., Wong, P., Zahn, R., Sasajala, P., *et al.* (2003) *J. Cell Sci.* **116,** 3957–3970.
14. Finken-Eigen, M., Rohricht, R. A. & Kohrer, K. (1997) *Curr. Genet.* **31,** 469–480.
15. Yoshimori, T., Yamagata, F., Yamamoto, A., Mizushima, N., Kabeya, Y., Nara, A., Miwako, I., Ohashi, M., Ohsumi, M. & Ohsumi, Y. (2000) *Mol. Biol. Cell* **11,** 747–763.
16. Bishop, N. & Woodman, P. (2000) *Mol. Biol. Cell* **11,** 227–239.
17. Scheuring, S., Rohricht, R. A., Schoning-Burkhardt, B., Beyer, A., Muller, S., Abts, H. F. & Kohrer, K. (2001) *J. Mol. Biol.* **312,** 469–480.
18. Dougan, D. A., Mogk, A., Zeth, K., Turgay, K. & Bukau, B. (2002) *FEBS Lett.* **529,** 6–10.
19. Scott, A., Chung, H.-Y., Gonciarz-Swiatek, M., Hill, G. C., Whitby, F. G., Gaspar, J., Holton, J. M., Viswanathan, R., Ghaffarian, S., Hill, C. P. & Sundquist, W. I. (2005) *EMBO J.*, in press.
20. Phillips, S. A., Barr, V. A., Haft, D. H., Taylor, S. I. & Haft, C. R. (2001) *J. Biol. Chem.* **276,** 5074–5084.
21. Ciccarelli, F. D., Proukakis, C., Patel, H., Cross, H., Azam, S., Patton, M. A., Bork, P. & Crosby, A. H. (2003) *Genomics* **81,** 437–441.
22. Reid, E., Connell, J., Edwards, T. L., Duley, S., Brown, S. E. & Sanderson, C. M. (2005) *Hum. Mol. Genet.* **14,** 19–38.
23. Letunic, I., Copley, R. R., Schmidt, S., Ciccarelli, F. D., Doerks, T., Schultz, J., Ponting, C. P. & Bork, P. (2004) *Nucleic Acids Res.* **32,** D142–D144.
24. Pearson, W. R. & Lipman, D. J. (1988) *Proc. Natl. Acad. Sci. USA* **85,** 2444–2448.
25. Garrus, J. E., von Schwedler, U. K., Pornillos, O. W., Morham, S. G., Zavitz, K. H., Wang, H. E., Wettstein, D. A., Stray, K. M., Cote, M., Rich, R. L., *et al.* (2001) *Cell* **107,** 55–65.
26. von Schwedler, U. K., Stray, K. M., Garrus, J. E. & Sundquist, W. I. (2003) *J. Virol.* **77,** 5439–5450.
27. Myszka, D. G. (1999) *J. Mol. Recognit.* **12,** 279–284.
28. Guntert, P. (2004) *Methods Mol. Biol.* **278,** 353–378.
29. Schubert, M., Labudde, D., Oschkinat, H. & Schmieder, P. (2002) *J. Biomol. NMR* **24,** 149–154.
30. Brunger, A. T., Adams, P. D., Clore, G. M., DeLano, W. L., Gros, P., Grosse-Kunstleve, R. W., Jiang, J. S., Kuszewski, J., Nilges, M., Pannu, N. S., *et al.* (1998) *Acta Crystallogr. D* **54,** 905–921.
31. Laskowski, R. A., Rullmannn, J. A., MacArthur, M. W., Kaptein, R. & Thornton, J. M. (1996) *J. Biomol. NMR* **8,** 477–486.
32. Crick, F. H. C. (1953) *Acta Crystallogr.* **6,** 689–697.
33. Walshaw, J. & Woolfson, D. N. (2001) *J. Mol. Biol.* **307,** 1427–1450.
34. Holm, L. & Sander, C. (1995) *Trends Biochem. Sci.* **20,** 478–480.
35. D'Andrea, L. D. & Regan, L. (2003) *Trends Biochem. Sci.* **28,** 655–662.
36. Fujita, H., Umezuki, Y., Imamura, K., Ishikawa, D., Uchimura, S., Nara, A., Yoshimori, T., Hayashizaki, Y., Kawai, J., Ishidoh, K., *et al.* (2004) *J. Cell Sci.* **117,** 2997–3009.
37. Errico, A., Ballabio, A. & Rugarli, E. I. (2002) *Hum. Mol. Genet.* **11,** 153–163.
38. Trotta, N., Orso, G., Rossetto, M. G., Daga, A. & Broadie, K. (2004) *Curr. Biol.* **14,** 1135–1147.
39. Patel, H., Cross, H., Proukakis, C., Hershberger, R., Bork, P., Ciccarelli, F. D., Patton, M. A., McKusick, V. A. & Crosby, A. H. (2002) *Nat. Genet.* **31,** 347–348.
40. Lin, Y., Kimpler, L. A., Naismith, T. V., Lauer, J. M. & Hanson, P. I. (2005) *J. Biol. Chem.* **280,** 12799–12809.
41. Wolf, E., Kim, P. S. & Berger, B. (1997) *Protein Sci.* **6,** 1179–1189.
42. Cornilescu, G., Delaglio, F. & Bax, A. (1999) *J. Biomol. NMR* **13,** 289–302.